

## AERODYNAMIC PERFORMANCE ANALYSES OF ICED TURBINE BLADE PROFILE WITH TRANSITIONAL DDES

Özgür Yalçın\*  
Middle East Technical University  
Ankara, Turkey

Özcan Yırtıcı†  
Osmaniye Korkut Ata University  
Osmaniye, Turkey

Yusuf Özyörük‡ and İsmail H.  
Tuncer§  
Middle East Technical University  
Ankara, Turkey

### ABSTRACT

*Ice accretion on wind turbine blades changes the initial shape which alters the aerodynamic characteristics unfavorably. In this study, performance degradation on blades due to rime ice shape, which is predicted well by the presented method, is analyzed by delayed detached-eddy simulation (DDES) using two different subgrid length scales: a maximum cell edge and a shear-layer-adapted (SLA) length. As a turbulence model, Spalart-Allmaras equation with and without a zero-equation algebraic transition model (B-C model) is used. The results of iced blade profiles, compared with measured data, show DDES with SLA subgrid length scale captures stall behavior in more accuracy than standard DDES. On the other side, B-C model has no certain favorable effect around the stall angles.*

### INTRODUCTION

Wind resources in cold climate regions and highlands are typically good and making them attractive for wind energy. However, the formation of ice on wind turbine blades degrades the aerodynamic performance. One example is the rime ice shape, which typically forms at temperatures from 0 °C down to -40 °C. This kind of ice has a milky, opaque appearance with smooth shapes, tends to grow into the air-stream, and can be easily removed by de-icing or prevented by anti-icing systems. It usually occurs at low airspeed, low temperature and low liquid water content. Rime ice accretion causes different boundary layer transition onset and separation region over the turbine. Early stall behavior, depending on the ice shape, might be observed undesirably. Consequently, having a numerical solver that can handle all flow regimes such as laminar flow, laminar-turbulent transition, and fully turbulent flow is essential for accurate wind turbine blade simulations.

\*GRA in Aerospace Engineering Department, Email: oyalcin@ae.metu.edu.tr

†GRA in Graduate School of Natural and Applied Sciences, Email: ozcanyirtici@osmaniye.edu.tr

‡Prof. in Aerospace Engineering Department, Email: yusuf.ozyoruk@ae.metu.edu.tr

§Prof. in Aerospace Engineering Department, Email: ismail.h.tuncer@ae.metu.edu.tr

Delayed detached-eddy simulation (DDES), in recent years, has been widely used by both industry and academic communities because it can supply high accuracy with low computational costs in wall-bounded aerodynamic problems. However, as the name infers DDES is good at massively separated flows, not at all flow regimes. It has been shown in the study of [Yalçin et al., 2018] that DDES with shear-layer-adapted (SLA) subgrid length scale, proposed by [Shur et al., 2015], could reveal a laminar separation bubble inside boundary layer and capture boundary layer transition phenomena along the NREL S826 wind turbine blade profile unlike standard DDES one. SLA length scale simply detects Kelvin-Helmholtz instability inside shear-layers, then reduces the subgrid length scale, and accelerates transition from RANS mode to LES mode of DES eventually. However, prediction of an exact location of the transition onset requires an additional transition model. In the scope of this study, transitional DDES is aimed by combining SLA length scale and Bas-Cakmakcioglu (B-C) transition model [Cakmakcioglu et al., 2018]. B-C is a zero-equation algebraic transition model. It simply multiplies an intermittency function depending on local turbulent information with the production term of the Spalart-Allmaras (S-A) equation, and thereby provides a boundary layer transition prediction. In this study, a rime ice accretion around the surface of a blade having NACA 23012 profile is predicted by the method presented in reference [Yirtici et al., 2019]. Then, flow with Reynolds number of  $1.8 \times 10^6$  and Mach number of 0.18 over the iced blade is simulated with different DDES approaches: standard DDES, DDES with SLA, DDES with B-C model, and DDES with SLA and B-C model. The simulations have been performed for the angles of attack around stall regions. For the simulations, an inhouse solver, METUDES developed for aeroacoustic purposes in Aerospace Engineering Department in METU [Cengiz, 2018], is used. The remaining part of this paper firstly presents ice accretion prediction methodology as well as DDES formulation with SLA length scale and B-C transition model. Then, it is continued with the validation of these methods. Finally, the aerodynamic results of NACA 23012 with rime ice shape are demonstrated with comparisons to the experimental data of [Broeren et al., 2014] which provides sufficient 3-D ice accretion measurements.

## METHODOLOGY

### Ice Accretion Prediction

Ice accretion prediction involves complex physics comprising aerodynamics, heat transfer and multi-phase flow, which are all time dependent and involve geometric deformation. The numerical method employed in this study predicts the ice accretion on aerodynamic surfaces as a result of water droplets hitting on the surface iteratively. It employs the general methodology for the simulation of ice accretion on airfoils, which is based on the successive calculation of air flow, water droplet trajectories, collection efficiency, heat transfer balance and accreted ice. In order to determine the flow field velocity components for droplet trajectory calculations, Hess-Smith panel method is used. Droplet trajectories are computed by using a Lagrangian approach to obtain the collection efficiency distribution around the airfoil. To determine the thickness of ice, convective heat transfer coefficients are determined by using the two-dimensional Integral Boundary Layer equation and the thermodynamic balance is achieved with the Extended Messinger model. Extended Messinger Model is governed by four equations; energy equations in ice and water layers, a mass balance and a phase change or Stefan condition at the ice/water interface [Myers, 2001].

$$\frac{\partial T}{\partial t} = \frac{k_i}{\rho_i C p_i} \frac{\partial^2 T}{\partial y^2} \quad (1)$$

$$\frac{\partial \theta}{\partial t} = \frac{k_w}{\rho_w C p_w} \frac{\partial^2 \theta}{\partial y^2} \quad (2)$$

$$\rho_i \frac{\partial B}{\partial t} + \rho_w \frac{\partial h}{\partial t} = \rho_a \beta V_\infty \quad (3)$$

$$\rho_i L_F \frac{\partial B}{\partial t} = k_i \frac{\partial T}{\partial y} - k_w \frac{\partial \theta}{\partial y} \quad (4)$$

where  $\theta$  and  $T$  are the temperatures,  $k_i$  and  $k_w$  are thermal conductivities,  $Cp_i$  and  $Cp_w$  are the specific heats and  $h$  and  $B$  are the thickness of water and ice layers, respectively. In equation 3,  $\rho_a \beta V_\infty$  is impinging water mass flow rates for a panel, respectively. Meanwhile,  $\rho_i$  and  $L_F$  refer the density of ice and the latent heat of solidification of water. In order to determine the ice and water thicknesses together with the temperature distribution at each layer, boundary and initial conditions must be specified. These are based on the following assumptions [Myers, 2001]:

- Ice is in perfect contact with the airfoil surface, which is taken to be equal to the air temperature,  $T_a$ :

$$T(0, t) = T_s \quad (5)$$

- The temperature is continuous at the ice/water boundary and is equal to the freezing temperature:

$$T(B, t) = \theta(B, t) = T_f \quad (6)$$

- At the air/water (glaze ice) or air/ice (rime ice) interface, heat flux is determined by convection ( $Q_c$ ), radiation ( $Q_r$ ), latent heat release ( $Q_l$ ), cooling by incoming droplets ( $Q_d$ ), heat brought in by runback water ( $Q_{in}$ ), evaporation ( $Q_e$ ) or sublimation ( $Q_s$ ), aerodynamic heating ( $Q_a$ ) and kinetic energy of incoming droplets ( $Q_k$ ):

$$\text{For glaze ice: } -k_w \frac{\partial \theta}{\partial y} = (Q_c + Q_e + Q_d + Q_r) - (Q_a + Q_k + Q_{in}) \quad \text{at } y = B + h \quad (7)$$

$$\text{For rime ice: } -k_i \frac{\partial T}{\partial y} = (Q_c + Q_s + Q_d + Q_r) - (Q_a + Q_k + Q_{in} + Q_l) \quad \text{at } y = B \quad (8)$$

- Airfoil surface is initially clean:

$$B = h = 0, \quad t = 0 \quad (9)$$

Detailed information about this methodology can be found in References [Özgen and Canibek, 2009; Ozgen and Canibek, 2010].

### Flow Solver, METUDES

METUDES [Cengiz, 2018], is a time-accurate, compressible, Navier-Stokes solver. The modified S-A turbulence one equation [Crivellini and D'Alessandro, 2014] is used for closure. It provides setting initial eddy viscosity in whole computational domain as zero; hence, simulations start as laminar flow everywhere. The resolution and modeling of turbulent structures are made using DDES approaches. The spatial discretization is performed by a fourth-order low-dissipation low-dispersion finite volume approach defined on 3-D curvilinear grids. The temporal discretization is the preconditioning-squared approach which makes use of dual-time stepping together with a low Mach number preconditioning and matrix time stepping.

### Transitional DDES

Transitional behavior for DDES is provided by combining SLA subgrid length scale and B-C transition model. Both methods are simply presented as follows:

B-C transition model: Boundary layer transition phenomena inside RANS region of DDES is aimed to be captured by a transition model. Bas-Cakmakcioglu (B-C) model is a zero-equation algebraic model [Cakmakcioglu et al., 2018], which is based on the S-A turbulence equation. It multiplies an intermittency function depending on local flow information with the production term of the S-A equation. The standard S-A one equation model slightly modified by B-C model is in the following form (in non-conservation form and without trip term):

$$\frac{\partial \tilde{\nu}}{\partial t} + \mathbf{V} \cdot \nabla \tilde{\nu} = \Psi + \gamma_{BC} \Pi - \Phi \quad (10)$$

where  $\tilde{\nu}$  is the eddy viscosity related term, and  $\mathbf{V}$  is the velocity vector of the flow field. The terms on the right hand side of Eq.10 represent diffusion, production and destruction, respectively. Here,  $\gamma_{BC}$ , the proposed intermittency distribution function, is given as

$$\gamma_{BC} = 1 - \exp(-\sqrt{Term_1} - \sqrt{Term_2}) \quad (11)$$

This function, having values from 0 to 1, hampers the production of eddy viscosity until some transition criteria is met. The terms are given as

$$Term_1 = \frac{\max(Re_\theta - Re_{\theta c}, 0.0)}{\chi_1 Re_{\theta c}}, \quad Term_2 = \frac{\max(\nu_{BC} - \nu_{cr}, 0.0)}{\nu_{cr}} \quad (12)$$

where

$$Re_\theta = \frac{Re_v}{2.193}, \quad Re_v = \frac{\rho d_w^2 \Omega}{\mu}, \quad \nu_{BC} = \frac{\nu_t}{U d_w}, \quad \nu_{cr} = \frac{\chi_2}{Re} \quad (13)$$

and  $\chi_1 = 0.002$ ,  $\chi_2 = 5.0$  are the calibration constants. The critical momentum thickness  $Re_{\theta c}$  is found from empirical correlations.

SLA subgrid length scale: DDES basically uses a switch between its RANS and LES modes during the computation of model length scale, which is the closest wall distance ( $d_w$ ) for the S-A equation.

$$l_{DDES} = l_{RANS} - f_d \max(0, l_{RANS} - l_{LES}) \quad (14)$$

where

$$l_{RANS} = d_w \quad (15)$$

$$l_{LES} = C_{DES} \Delta \quad (16)$$

$$f_d = 1 - \tanh([8r_d]^3) \quad (17)$$

$$r_d = \frac{\nu_t + \nu}{(U_{i,j} U_{i,j})^{0.5} \kappa^2 d_w^2} \quad (18)$$

The coefficient  $C_{DES} = 0.65$  has been set as a calibration constant based on decaying isotropic turbulence. Here, the classical DDES takes the subgrid length scale as  $\Delta = \Delta_{max} = \max(\Delta x, \Delta y, \Delta z)$ . A known weakness of DDES is that development of instabilities is delayed because of damping effects of the RANS model, such that transition to the LES mode is not rapid enough. On the other hand, shear-layer-adapted (SLA) subgrid length scale [Shur et al., 2015] accelerates the activation of LES mode in case of instabilities. It consists of redefinition of the subgrid length scale that not only depends on the grid but also on the flow, and its three-dimensionality. Firstly, a vorticity dependent subgrid length scale is defined:

$$\tilde{\Delta}_\omega = \frac{1}{\sqrt{3}} \max_{n,m=1,8} |\mathbf{I}_n - \mathbf{I}_m| \quad (19)$$

where  $\mathbf{I}_n = \mathbf{n}_\omega \times \mathbf{r}_n$ , and  $\mathbf{n}_\omega$  is the unit vorticity vector, while  $\mathbf{r}_n$  is the position vector for the vertices of the cell ( $n = 1, \dots, 8$  for hexahedral cells). This formulation removes dependency of subgrid viscosity on cell length (mostly  $\Delta_{max} = \Delta z$  for a shear layer in  $xy$  plane) in vorticity direction, which had been a problem in shear layers where the planar shear is expected to initiate transition to the LES mode. Instead, the subgrid viscosity is based on the maximum dimension on the shear plane in a quasi-2D region. Still, the resulting reduction of the subgrid viscosity is not sufficient to initiate the transition in quasi-2D regions. An ILES(improved large-eddy simulation)-like behavior is desired in such regions to allow K-H instabilities to take over. The so-called "Vortex Tilting Measure" (VTM) is defined to detect such regions,

$$VTM = \frac{\sqrt{6} |(\hat{\mathbf{S}} \cdot \boldsymbol{\omega}) \times \boldsymbol{\omega}|}{\omega^2 \sqrt{3 \text{tr}(\hat{\mathbf{S}}^2) - [\text{tr}(\hat{\mathbf{S}})]^2}} \quad (20)$$

It yields zero when the vorticity is aligned with any eigenvectors of the strain; nonzero when the deformation tensor tilts the vorticity vector.  $VTM$  is facilitated in the function

$$F_{KH}(\langle VTM \rangle) = \max \left[ F_{KH}^{min}, \min \left\{ F_{KH}^{max}, F_{KH}^{min} + \frac{F_{KH}^{max} - F_{KH}^{min}}{a_2 - a_1} (\langle VTM \rangle - a_1) \right\} \right] \quad (21)$$

where the angle brackets,  $\langle \cdot \rangle$ , means the value is averaged among neighboring cells. Averaging is necessary for smoothing the distribution since it is reported that  $VTM$  may have downward excursions locally.  $F_{KH}$  function is a simplistic function depending on  $VTM$  with the sole purpose of reducing the subgrid viscosity properly.  $F_{KH}^{max} = 1$  recovers the original length scale while  $F_{KH}^{min} = 0.1$ , and  $a_1 = 0.15$ ,  $a_2 = 0.3$  are constants adjusted through numerical experiments. Accordingly,  $F_{KH}$  varies linearly between  $\langle VTM \rangle = 0.15$  and  $\langle VTM \rangle = 0.3$  yielding values ranging from 0.1 to 1. Hence, the ultimate subgrid length scale is calculated by

$$\Delta_{SLA} = \tilde{\Delta}_\omega F_{KH}(\langle VTM \rangle) \quad (22)$$

The resulting length scale serves as a reduction to the vorticity-oriented length scale,  $\tilde{\Delta}_\omega$ , up to one order in regions where K-H instabilities are expected to occur, thus leaving ground to transition to resolved 3-D turbulent mode. However, for wall bounded flows, this reduction should be inactivated to keep the boundary layer shielded as done in standard DDES with  $\Delta_{max}$ . The following limitation to  $F_{KH}$  was proposed for that purpose,

$$F_{KH}^{lim} = \begin{cases} 1.0, & f_d < 0.99 \\ F_{KH}, & f_d \geq 0.99 \end{cases} \quad (23)$$

As a result, this version of DDES has proven success (by [Shur et al., 2015]) not only in free shear layers, but also in wall bounded flows, jet flows, decaying turbulence, and backward facing step flows.

## RESULTS AND DISCUSSION

### Validation Cases

Ice Accretion Prediction over NACA 0012 Wing Profile: The iced prediction method developed is validated against the experimental and numerical studies over NACA 0012 airfoil performed by Wright et al. [Wright et al., 1997].

The geometric and flow conditions in the reference study are presented in Table 1.

Table 1: Geometric characteristics and flow conditions used in the calculations

| Variables                       | Value                |
|---------------------------------|----------------------|
| Ambient temperature, $T_a$      | -27.8 °C             |
| Freestream velocity, $V_\infty$ | 58.1 m/s             |
| Airfoil chord ,c                | 0.53 m               |
| Liquid water content, $\rho_a$  | 1.3 g/m <sup>3</sup> |
| Droplet diameter, $d_p$         | 20 μ m               |
| Exposure time, $t_{exp}$        | 480 s                |
| Ambient pressure, $p_\infty$    | 95610 Pa             |
| Angle of attack, $\alpha$       | 4.0°                 |
| Humidity                        | 100 %                |

In Fig.1, obtained ice shapes are compared with those obtained numerically by DRA, NASA and ONERA respectively. It is observed all the predictions agree fairly well with the experimental data.

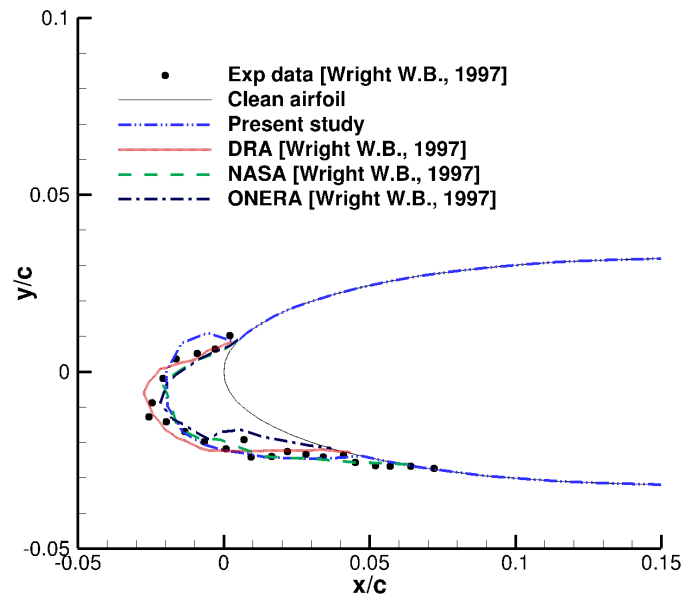


Figure 1: Comparison of ice shape predictions for NASA 27 case

Boundary Layer Transition Prediction over NREL S826 Blade Profile: Flow with Reynolds number of 145,000 and angle of attack of  $8^\circ$  is simulated around NREL S826 wind turbine blade profile by DDES with the standard subgrid length scale as well as with the SLA one. B-C model is also added and tested in the same problem. The results are compared with another studies [?] using DDES and  $k-\omega$  SST with Menter transition model, respectively, with 12 times finer grid domain than the current one. Fig.2 indicates that SLA length scale unlocks instability, and reveals a laminar separation bubble unlike the standard length scale. On the other hand, B-C zero-equation model predicted the laminar flow behavior before transition onset in more accuracy than all DDES studies. Fig.3 shows Q-criterion isosurfaces around the blade, which demonstrate vortical structures related to eddies. As seen, while standard DDES could capture mostly 2-D vortical structures, DDES with SLA accelerates the emergence of LES content even if flow is not fully turbulent.

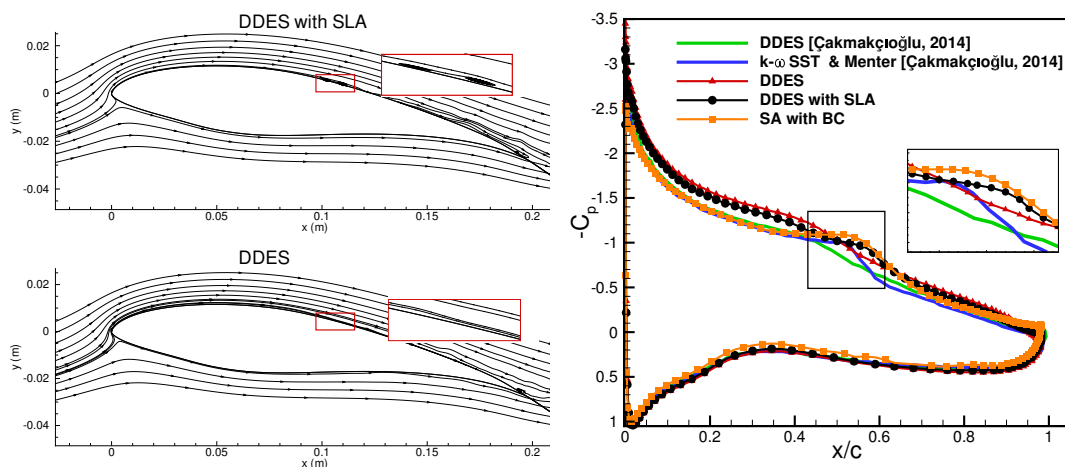


Figure 2:  $C_p$  distributions over the blade surface (left) and streamlines around the blade (right)

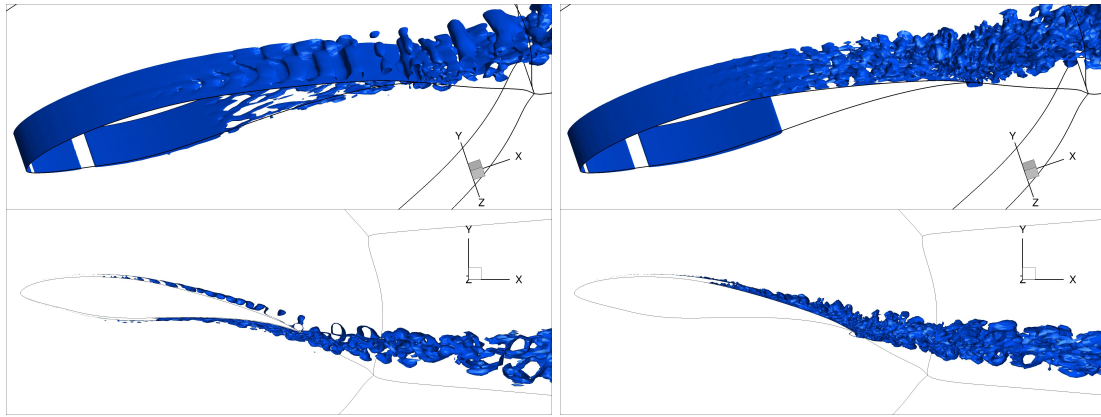


Figure 3: Isosurface of Q-criterion around the blade via DDES (left) and DDES with SLA (right)

### Flow over NACA 23012 with Rime Ice Shape

#### Ice shape prediction:

The ED1983-SLA ice roughness shape around 0.457 m-long blade with NACA 23012 profile, experimented in [Broeren et al., 2014], is predicted by the current method. The comparison is shown in Fig.4. This shape is known as a rime ice shape in literature. The prediction in general is good enough. A minor difference is occurred in the pressure side where the present method shows a straight line while a small step was observed in the experiment. The next thing is performing a flow simulation around the predicted iced profile.

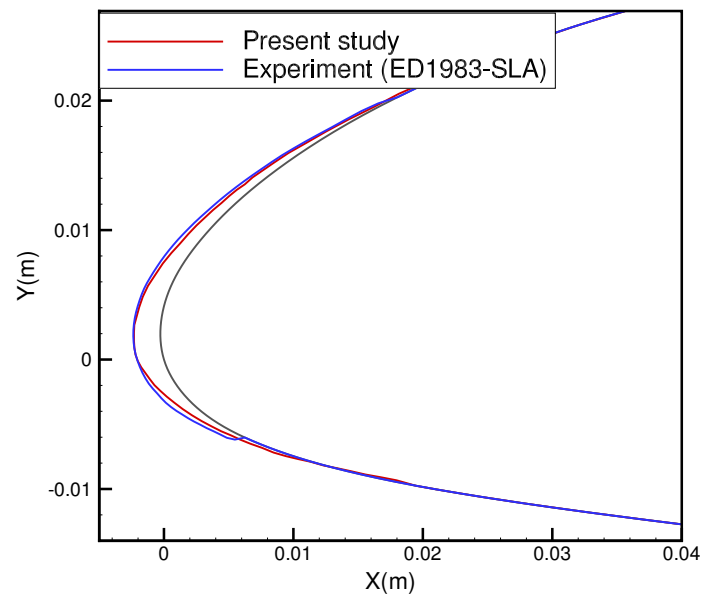


Figure 4: Comparison of ED1983-SLA ice roughness shape predicted by the current method with the measurement [Broeren et al., 2014]

#### Grid dependency study:

A tunnel grid is created around the blade profile. Fig.5 demonstrates the overset mesh topology with the boundary conditions. The chord length as well as the distance between upper and lower slip walls are the same as in the experiment. In the spanwise direction, periodic boundary condition is applied. Span is created by extrusion of 2-D domain. Span-to-chord length is chosen as 0.15 and totally 21 grid points are used which has been proven as sufficient for DES in the previous study [Yalçın et al.,

2018]. The O-mesh around the blade is the finest domain to resolve turbulent structures above the boundary layer. Grid dependency study is conducted with two meshes: Mesh A and Mesh B having O-mesh block with  $129 \times 79 \times 21$  grids and  $257 \times 79 \times 21$  grids, respectively. Only the grid points in the streamwise direction is changed because the resolution level by DES is affected by magnitudes of cell lengths near the boundary layer edge and corresponding maximum lengths are the ones in the streamwise direction. Fig.6 shows pressure coefficient distribution along the surface of clean NACA 23012 profile with angle of attack of  $9.3^\circ$ . The results are obtained by DDES with SLA simulations with two meshes as well as the measurement. Both mesh results differ from the experiment near the trailing edge. The reason might be the sharpness of the trailing edge is rounded during the mesh generation. On the other hand, the results of finer mesh (Mesh B), near the leading edge where the iced shape is observed, is in very good agreement with measured data unlike the coarse one (Mesh A). Hence, the remaining simulations are performed with mesh B. Note that the number of the total grid points including all five blocks is approximately 580,000.

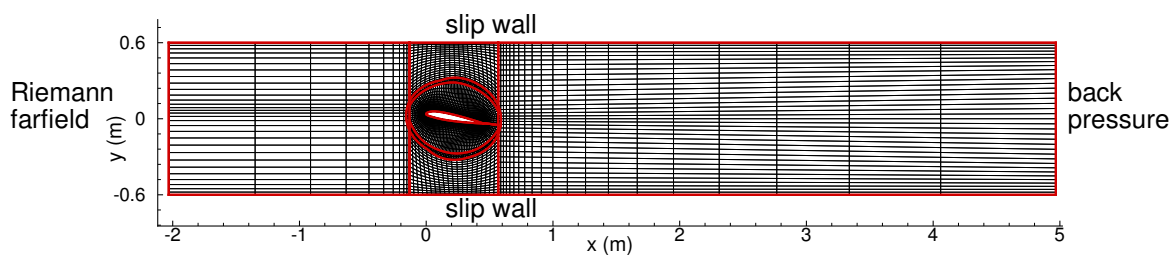


Figure 5: Full view of the tunnel grid (only the odd-numbered nodes are shown) with boundary conditions

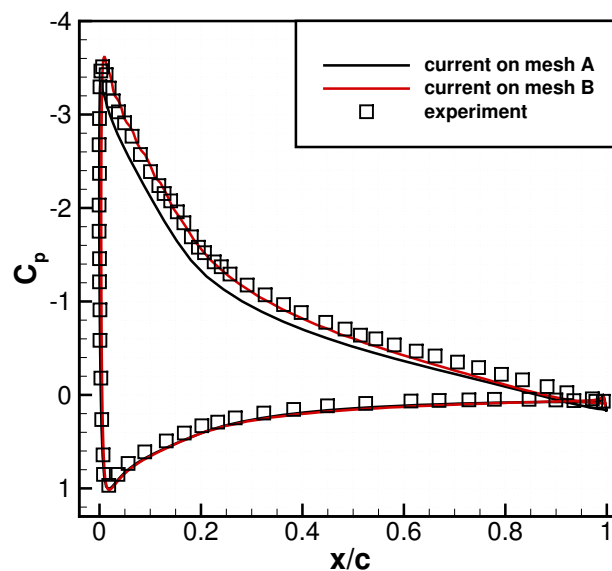


Figure 6: Comparison of  $C_p$  distributions over clean NACA 23012 profile obtained by DDES with SLA on both Mesh A (O-block with  $129 \times 79 \times 21$  nodes) and Mesh B (O-block with  $257 \times 79 \times 21$  nodes), and the experiment [Broeren et al., 2014]

#### Flow simulations using different DDES approaches:

The flow with Reynolds number of  $1.8 \times 10^6$  and Mach number of 0.18 is simulated using DDES with subgrid length scale as  $\Delta_{max}$  (referred as DDES) and  $\Delta_{SLA}$  (referred as DDES with SLA).

Some simulations are performed using the B-C transition model as well (referred as B-C & DDES, and B-C & DDES with SLA). The angles of attack are selected as  $8^\circ$ ,  $9.3^\circ$ ,  $12^\circ$ ,  $14^\circ$ , and  $16^\circ$  in order to analyze the stall behavior prediction of DDES. The unsteady simulations have been terminated when the running averages of aerodynamic coefficients are fixed.

Lift and drag coefficients ( $C_l$  and  $C_d$ ) are demonstrated in Fig.7. Before stall which happens around  $12^\circ$  in the experiment,  $C_l$  and  $C_d$  values obtained by all DDES studies are coincided perfectly with the measured data [Broeren et al., 2014]. Unfortunately, this is not the case after stall. Standard DDES results could not show the expected deviation trough the stall angle. Stall is observed after  $14^\circ$ , which is late when compared with the experiment. In the results of DDES with SLA, on the other side, a smooth stall occurred at the expected angle although it is deep in the experiment. The effect of B-C model to both subgrid length scales is not conclusive. It increased the  $C_l$  and decreased the  $C_d$  values in DDES approach. When it is added to DDES with SLA, B-C model did not have an impact much on the aerodynamic coefficients.

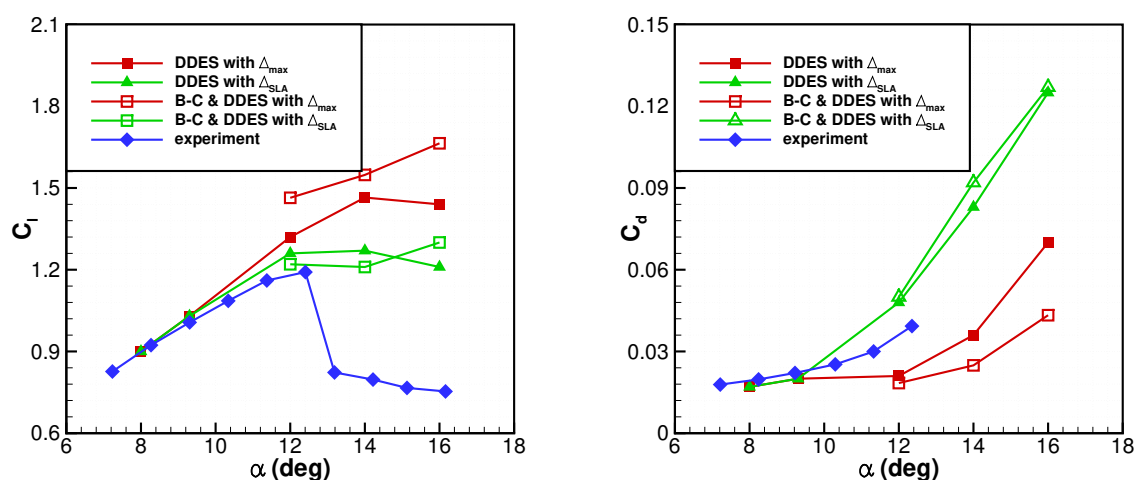


Figure 7: Comparisons of  $C_l$  and  $C_d$  values around stall region

Fig.8 shows the  $\tilde{\nu}/\nu$  contours of mean flow fields for angles of attack of  $12^\circ$ ,  $14^\circ$ , and  $16^\circ$ . The idea of resolving and modeling approaches of the presented methods is more clear when looking at the eddy viscosity contours. As expected, standard DDES keeps RANS functioning inside the attached boundary layer. When the flow is completely detached from the surface, it switches to the LES-mode and starts to resolve eddies. This is why the eddy viscosity values are reduced in the wake regions. In the case of  $\alpha = 16^\circ$ , the LES-mode is activated earlier because of massively separation along the surface where large eddies dominate. This is the typical behavior of DDES. On the other hand, SLA subgrid length scale accelerates the transition from modeled to resolution mode when it catches the instabilities inside the boundary layer. For all angles of attack, the eddy viscosity contours along the surface are weaker than those in the DDES studies. Consequently, DDES with SLA lets the instabilities continue and early stall can be observed before the massive separation happening. When the B-C transition model is included, the contours for all angles and models are remarkably changed. One favorable observation is that the eddy viscosity disappears at the pressure side for all cases. Unless instabilities trigger the laminar-turbulent transition, B-C model prevents the activation of production term of the S-A equation. However, it seems at the suction side B-C model breaks the balance between production and destruction terms during the RANS-LES switch. Hence, eddy contours are getting stronger and the simulations act as a sort of RANS even in the wake regions. This consequence is observed in mostly B-C & DDES results. SLA subgrid length scale effect seems to dominate the flow field more.

In order to see the turbulent structures around the blade explicitly, isosurfaces of Q-criterion are drawn

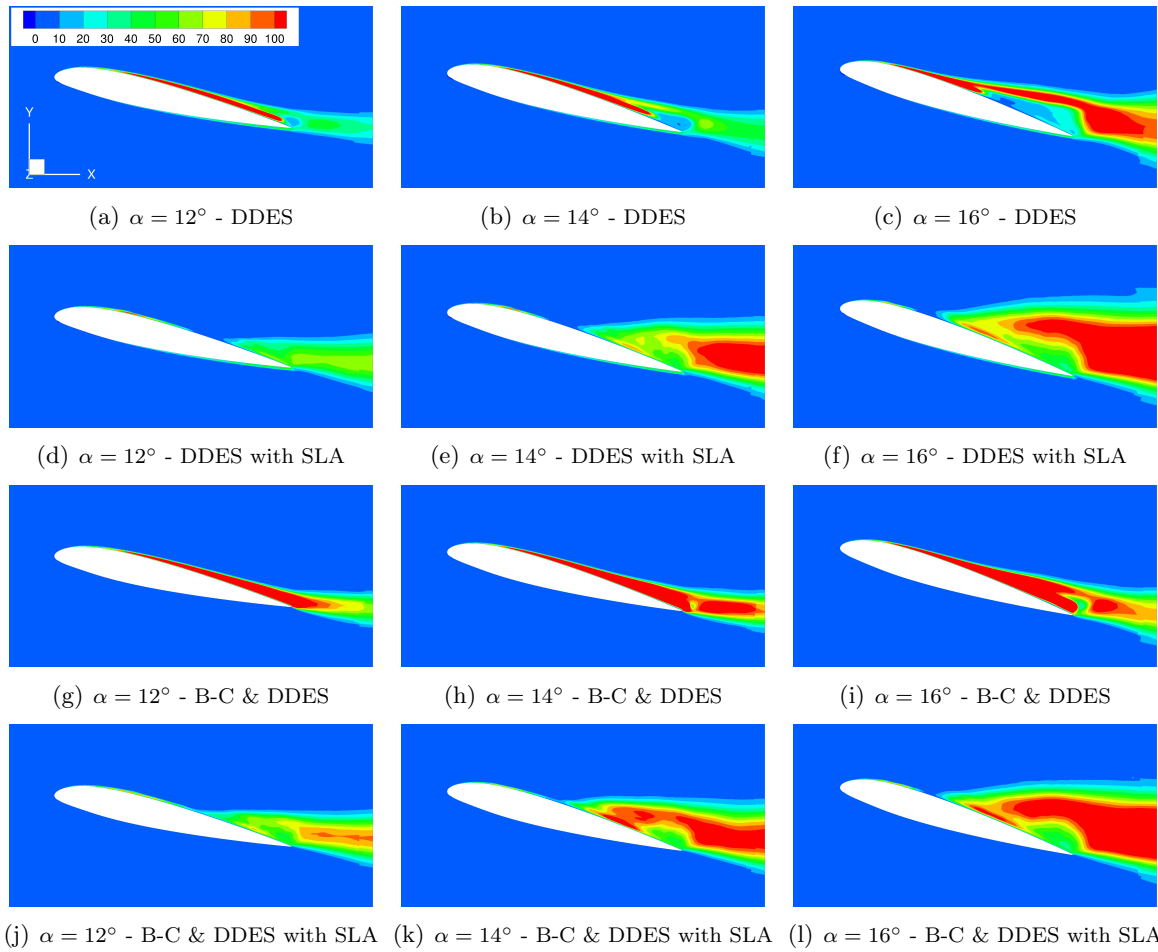


Figure 8:  $\tilde{\nu}/\nu$  contours of mean flow fields for different AoAs through different modeling approaches

in Fig.9. Subgrid length scale effect on isosurfaces is obvious. DDES approach mostly reveals 2-D vortical structures whereas a quick transition to LES-mode so as three dimensionality is obtained by DDES with SLA. Again, there is not much observable effect of B-C model on the isosurfaces when it is used with SLA length scale. But, an increment of the RANS functioning, an adverse effect on stall behavior, arises by B-C & DDES approaches.

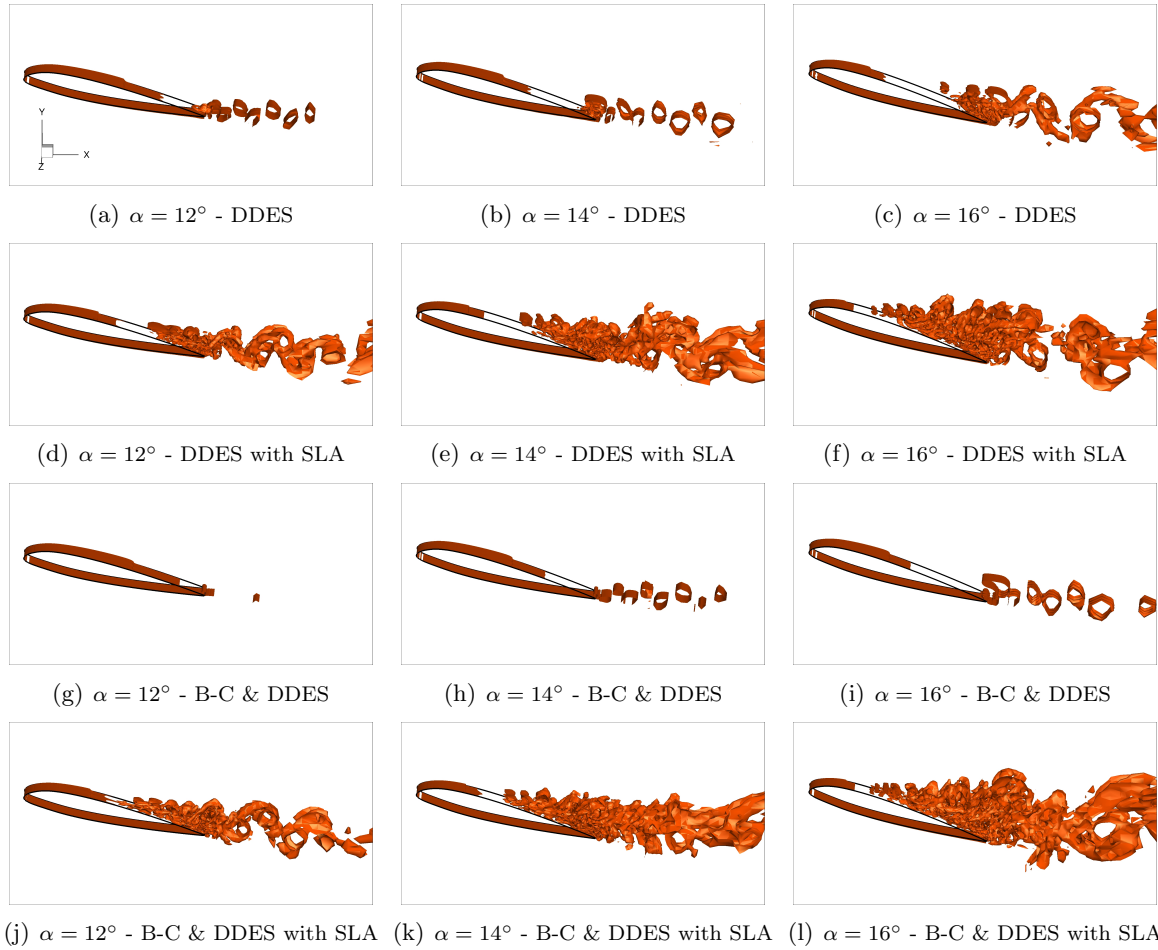


Figure 9: Isosurfaces of Q-criterion around the blade for different AoAs through different modeling approaches

## CONCLUSIONS

Flow over a NACA 23012 blade profile with rime ice accretion has been simulated by different DDES approaches. Rime ice shape over the surface was predicted accurately by the presented method. The results showed that DDES with the standard subgrid length scale,  $\Delta_{max}$ , is not capable to capture aerodynamic stall. However, using shear-layer-adapted subgrid length scale,  $\Delta_{SLA}$ , instead of the standard one can reveal a smooth stall behavior at the expected angle of attack although the correct lift and drag coefficients after stall are not captured. SLA length scale detects instabilities inside the boundary layer, and then reduces the eddy viscosity. This provides acceleration of transition to resolution mode (LES-mode). Hence, without any necessity of massive separation over the blade DDES with SLA can show earlier stall than standard DDES. A zero-equation Bas-Cakmakcioglu (B-C) transition model was also included in the simulations. It was shown that B-C model spoils the switching from RANS to LES-mode of DDES at the suction side while it provides laminar flow at the pressure side as expected. However, SLA length scale results are not affected by B-C model usage at the suction side; therefore, there occurs a slight improvement on the coefficients around the stall angles. As a result, DDES with SLA has a potential to capture stall behavior. It still requires an apparent transition model though transition model should be selected carefully considering the balance of RANS-LES switching.

## References

- Broeren, A. P., Addy, H. E., Lee, S., and Monastero, M. C. (2014). Validation of 3-d ice accretion measurement methodology for experimental aerodynamic simulation. In *6th AIAA Atmospheric and Space Environments Conference*, page 2614.
- Cakmakcioglu, S. C., Bas, O., and Kaynak, U. (2018). A correlation-based algebraic transition model. *Proceedings of the Institution of Mechanical Engineers, Part C: Journal of Mechanical Engineering Science*, 232(21):3915–3929.
- Cengiz, K. (2018). *Use of detached eddy simulation for aerodynamics and aeroacoustics of blade sections*. PhD thesis, Middle East Technical University.
- Crivellini, A. and D'Alessandro, V. (2014). Spalart–Allmaras model apparent transition and RANS simulations of laminar separation bubbles on airfoils. *International Journal of Heat and Fluid Flow*, 47:70–83.
- Myers, T. G. (2001). Extension to the messinger model for aircraft icing. *AIAA journal*, 39(2):211–218.
- Özgen, S. and Canibek, M. (2009). Ice accretion simulation on multi-element airfoils using extended messinger model. *Heat and Mass Transfer*, 45(3):305.
- Ozgen, S. and Canibek, M. (2010). In-flight icing simulation with supercooled large droplet effects. *HEFAT 2010*.
- Shur, M. L., Spalart, P. R., Strelets, M. K., and Travin, A. K. (2015). An enhanced version of des with rapid transition from rans to les in separated flows. *Flow, Turbulence and Combustion*, 95(4):709–737.
- Wright, W. B., Gent, R., and Guffond, D. (1997). Dra/nasa/onera collaboration on icing research. part 2; prediction of airfoil ice accretion.
- Yalçın, Ö., Cengiz, K., and Özyörük, Y. (2018). High-order detached eddy simulation of unsteady flow around nrel s826 airfoil. *Journal of Wind Engineering and Industrial Aerodynamics*, 179:125–134.
- Yirtici, O., Ozgen, S., and Tuncer, I. H. (2019). Predictions of ice formations on wind turbine blades and power production losses due to icing. *Wind Energy*, 22(7):945–958.